# Variational and Numerical Analysis of Contour-Based Segmentation Methods in Cephalometry

**Yulia Zh. Pchelkina**
Samara National Research University, 34 Moskovskoe shosse, Samara 443086, Russian Federation
*e-mail: pchelkina.yuj@ssau.ru

**Abstract.** A method for the automatic extraction of the soft-tissue facial profile contour is proposed, along with the detection of key cephalometric landmarks based on extremum analysis of a parameterized contour function and subsequent determination of the profile type and its harmony. A variational and numerical analysis of the influence of weighting coefficients in the energy functional on segmentation accuracy and diagnostic indicators is conducted, allowing the parameter selection to be justified and ensuring robust automatic annotation comparable to manual cephalometric analysis.

**Keywords:** variational methods; contour segmentation; image segmentation; model parameter analysis; orthodontics, cephalometry.

Paper #9561 received 26 Mar 2026; revised manuscript received 30 Apr 2026; accepted for publication 30 Apr 2026; published online 17 Jun 2026. doi: 10.18287/JBPE26.12.020309.

## 1 Introduction

Digital processing of biomedical images is one of the key directions in modern medical engineering, providing objectivity in diagnostics and reducing dependence on the subjective factor. One of the clinically significant applied tasks in this field is the automated cephalometric analysis of soft-tissue facial profile photographs, used in orthodontics and orthognathic surgery. During such analysis, the orthodontist evaluates both anatomical and aesthetic characteristics of the patient's face, including face shape, soft-tissue proportions, and possible dentofacial anomalies. These data are recorded in the descriptive section of the photo protocol and serve as an important basis for diagnosis, treatment planning, and subsequent outcome evaluation [1].

Currently, the identification of key cephalometric landmarks on photographs, measurement of angles and linear dimensions, and computation of derived anthropometric characteristics are typically performed manually. This approach is time-consuming, places high demands on specialist qualification, and is subject to subjectivity, which may lead to measurement variability between different clinicians and between repeated measurements of the same case.

Automation of biomedical facial image analysis allows measurements to be standardized, examination time to be reduced, and human error to be minimized – which is especially important when processing large clinical datasets and preparing training samples for intelligent diagnostic systems. The task of facial contour extraction and cephalometric landmark localization is addressed using computer vision and digital image processing methods – from simple threshold-based approaches to complex variational and machine-learning models. The choice of algorithm is determined by accuracy requirements: in cephalometric tasks, correct extraction of the soft-tissue boundary and precise landmark positioning are critical, since even small errors can affect profile type classification and facial harmony assessment. Therefore, the active contour variational method is chosen in this work as the primary tool for soft-tissue profile extraction, enabling iterative deformation of an initial contour until it coincides with the actual object boundary, thus ensuring the required accuracy and robustness of biomedical segmentation.

## 2 Anthropometric Analysis of the Facial Profile

Anthropometric analysis of the facial profile is based on a geometric description of the relative positions of key cephalometric landmarks located on the soft-tissue facial contour. Within the classical approach, profile type assessment is performed by measuring the angle between two lines passing through predefined reference points. These lines model the general contour of the frontonasal and nasal-chin segments of the profile and allow quantitative characterization of the degree of convexity or concavity of the facial profile relative to a conventional neutral (straight) configuration.

Standard cephalometric landmarks are used as reference points. The Gl point (glabella) is defined as the most anteriorly projecting point of the forehead in the sagittal plane and serves as an orientation point for the upper facial segment. The Sn point (subnasale) is located at the junction of the nasal septum skin and the upper lip, reflecting the transition from the nasal to the labial segment. The Pg point (pogonion) corresponds to the maximum anterior projection of the soft-tissue chin and characterizes the distal facial segment. Together, these points form the minimally sufficient set for a primary angular assessment of facial profile shape.

The angle between the lines drawn through these points is interpreted in terms of three main profile types in anthropometric analysis. The profile is considered straight if the measured angle is close to 180°, indicating a balanced position of the frontal, nasal, and chin segments without pronounced prognathia or retrognathia. If the angle is less than 170°, the profile is classified as convex; this configuration is typically associated with relative protrusion of the midface or chin retrognathia. When the angle exceeds 170°, the profile is assessed as concave, which generally reflects relative anterior displacement of the chin or a flatter midface position [2].

Additionally, the Ricketts aesthetic line is widely used in aesthetic profile analysis. It is defined as the line connecting the tip of the nose and the most prominent point of the chin. The position of the lips relative to this line serves as a qualitative and quantitative criterion of soft-tissue profile harmony (Fig.1).

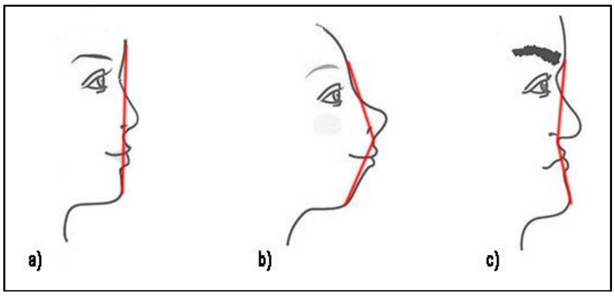


Fig. 1 Facial profile types: a) straight profile, b) convex profile, c) concave profile.

The profile is considered harmoniously developed when the aesthetic line does not intersect the lip contour and the lips either touch it or are positioned within the acceptable posterior deviation (the upper lip is 2–3 mm posterior to this line, the lower lip is 1–2 mm posterior). This state is interpreted as a sign of balanced facial proportions and compliance with accepted aesthetic norms. A disharmonious profile is almost always associated with dentofacial anomalies and carries not only aesthetic but also functional problems requiring various orthodontic interventions depending on the profile type [3].

## 3 Contour Extraction Method

For contour extraction in an image, the segmentation task is formulated as variational minimization of the energy functional of a curve defined on the image plane. Let $I(x, y)$ – be the scalar intensity field of the source image, and let the closed contour $C$ be given in parametric form:

$$C(s) = \big(x(s), y(s)\big),\ s \in [0, 1].$$

The contour behavior is then described through the total energy, which depends both on its own geometry and on the image properties in the neighborhood of the contour points.

In the discrete formulation used in this work, the initial contour is represented as an ordered set of vertices $\{v_i\}_{i=1}^{n}$, where $v_i = (x_i, y_i)$ and $n$ is the number of vertices. The contour iteratively changes its shape until it approximates the object geometry to a specified accuracy [4–6]. For each vertex $v_i$ a scalar energy is introduced:

$$E_i(v_i) = a \cdot E_{int}(v_i) + b \cdot E_{ext}(v_i),$$

where $E_{int}(v_i)$ is the contribution of the internal (geometric) energy depending on the contour shape and smoothness in the neighborhood of $v_i$; $E_{ext}(v_i)$ is the contribution of the external energy determined by the image structure $I(x, y)$ in the neighborhood of $v_i$; $a$ and $b > 0$ are weighting coefficients regulating the balance between regularization and boundary attraction.

To obtain the object contour, the total energy is minimized:

$$\sum_{i=1}^{n} E_i(v_i).$$

Minimization is performed iteratively: at each step, each contour vertex $v_i$ moves to the position corresponding to a reduction of local energy $E_i$ Deformation continues until changes in energy and/or vertex positions fall below a specified threshold, which is interpreted as reaching an approximate local minimum of the functional.

The energy functions in this model are defined in discrete form and interpreted as matrices (or window filters) defined in the neighborhood of each contour point. The central element of such a matrix corresponds to the value of the chosen energy function computed directly at the contour point. The remaining elements contain values of the same energy function for a set of points belonging to a local neighborhood of that point in the image. Thus, each energy function is described not only at a single point but in a neighborhood of $v_i$, allowing the local image structure to be taken into account when evaluating energy and updating the contour.

The internal energy affects the shape and smoothness of the contour and is designed to constrain contour shape, preventing jaggedness and unnatural oscillations. It models the elastic-rigid properties of the curve. In discrete notation, the internal energy is represented as a combination of two components:

$$a \cdot E_{int}(v_i) = \mathrm{c} \cdot E_{con}(v_i) + d \cdot E_{bal}(v_i),$$

where $E_{con}(v_i)$ is the smoothing energy (configurational energy controlling distances and relative positions of neighboring vertices), $E_{bal}(v_i)$ is the so-called balloon (bursting) energy responsible for displacing the contour outward or inward relative to the object; $c,\ d > 0$ are the corresponding weighting coefficients.

Elements of the smoothing energy matrix for a closed contour are computed as:

$$e_{jk}(v_i) = \frac{n}{\sum_{i=1}^{n}|v_{i+1}-v_i|^2} \cdot \left| p_{jk}(v_i - \frac{v_{i-1}+v_{i+1}}{2cos\,(\frac{2\pi}{n})}) \right|^2,$$

where $p_{jk}(v_i)$ are the neighborhood points of $v_i$ in the image (discrete mask around the vertex), $n$ is the number of contour vertices. This formula implements a discrete approximation of the second derivative (curvature) of the curve accounting for its cyclic (closed) structure: the expression

$$(v_{i-1} + v_{i+1})/2\,cos\left(\frac{2\pi}{n}\right)$$

defines the "expected" vertex position for uniformly distributed points on a circle, and the magnitude of the difference with the actual position $p_{jk}(v_i)$ measures the degree of local deviation from a smooth configuration.

The normalization factor $n/\sum_{i=1}^{n}|v_{i+1} - v_i|^2$ makes the smoothing energy invariant to the overall scale of the contour: dividing by the total squared arc length ensures that $E_{con}$ does not grow simply because the contour is large, allowing the weighting coefficient $c$ to be interpreted independently of image resolution.

The factor $1/(2cos(2\pi/n))$ arises from the expected position of a vertex on a regular $n$-gon inscribed in a circle: for equally spaced points, the midpoint of the neighbors $(v_{i-1} + v_{i+1})/2$ lies at distance $r\,cos(2\pi/n)$ from the centre, where $r$ is the polygon radius. This term serves as a discrete normalisation ensuring that the smoothing energy vanishes for a uniformly sampled circle.

The balloon energy $E_{bal}(v_i)$ deforms the contour in one direction, is introduced to control the radial displacement of the contour relative to the object, and can be written as:

$$e_{jk}(v_i) = n_i\left(v_i - p_{jk}(v_i)\right),$$

where $n_i$is the vector defining the preferred deformation direction (e.g., the normal to the contour at $v_i$), and $p_{jk}(v_i)$ are the neighborhood points relative to which the displacement is assessed. Thus, the internal energy defines a nonlocal regularizing term ensuring contour robustness to noise and small artifacts.

The external energy is responsible for attracting the contour to object boundaries detected by brightness and gradient characteristics of the image. In the model used, it takes the form:

$$a \cdot E_{ext}(v_i) = g \cdot E_{mag}(v_i) + h \cdot E_{grad}(v_i),$$

where $E_{mag}(v_i)$ reflects the contribution of absolute brightness values, and $E_{grad}(v_i)$ is the contribution of the brightness gradient magnitude; $g,\ h > 0$ are weighting coefficients regulating the role of each factor.

Elements of the image energy matrix $E_{mag}(v_i)$ are defined directly by brightness:

$$e_{jk}(v_i) = I\left(p_{jk}(v_i)\right),$$

meaning the darker (or, depending on the convention chosen, the brighter) the region, the lower (or higher) its energy contribution.

Elements of the gradient energy matrix $E_{grad}(v_i)$ are defined as:

$$e_{jk}(v_i) = -\left|\overline{\nabla I}\left(p_{jk}(v_i)\right)\right|,$$

where $\overline{\nabla I}$ is the discrete brightness gradient at point $p_{jk}(v_i)$, representing a two-dimensional vector of partial derivatives in the vertical and horizontal directions. The negative sign ensures contour attraction to regions with high gradient magnitude (boundaries), since such points yield minimum energy.

Together, the parameters $a$, $b$, $c$, $d$, $g$, $h$ define the weighting coefficients in the generalized energy functional and allow fine-tuning the trade-off between contour smoothness and accuracy of fit to the object boundary. With correct selection of these coefficients, the resulting contour approximates the desired facial boundary with the required degree of accuracy and robustness to noise and illumination variations [7].

Total energy minimization is performed using the greedy algorithm. At each iteration, the algorithm sequentially processes all $n$ contour vertices. For each vertex $v_i$, a discrete neighborhood $N(v_i)$ is formed – a discrete mask of size $(2s + 1) \times (2s + 1)$ pixels, where parameter $s$ defines the search radius. Within this neighborhood, values of all energy functional components are computed, and the vertex is moved to the point with the minimum total local energy. If the neighborhood center is already the minimum (the vertex did not move), a "fixed point" is recorded, which is used in the stopping criterion. The procedure repeats until the stopping criterion is met: iterations cease if the fraction of fixed vertices in one iteration exceeds threshold $\theta_{stop}$, or the change in total energy $|E^t\ -\ E^{\{t-1\}}|$ becomes less than a specified $\varepsilon$, or the maximum number of iterations $T_{max}$ is reached. The greedy algorithm has computational complexity $O(nm)$, which is more than an order of magnitude faster than the dynamic programming approach with complexity $O(nm^3)$.

# 4 Contour Extraction for Facial Profile Detection

In most applications of the described contour method, the initial contour is set manually by the user. To automate this step, pre-trained face detection models are used: a

Haar cascade classifier or the Dlib model [8, 9]. The center of the detected facial region serves as the center of the initial circular contour.

An important role in active contour methods is played not only by initial contour placement and image preprocessing, but also by parameter selection. The parameters $a$, $b$, $c$, $d$, $g$, $h$ should be chosen to balance the contributions of internal and external energies: the contour must be sufficiently smooth while also being close to the real object boundary. In practice, it is necessary to determine the relative weights of different terms in the energy functional and find ratios at which the minimum of this functional yields the desired contour [10].

From a mathematical analysis perspective, the following key selection principles should be considered:

**1 Energy normalization.** It is advisable to first estimate the magnitudes of the energy functions on test images by computing the mean or median value of each energy across contour points and multiple images: $\bar{E}_{con}, \bar{E}_{bal}, \bar{E}_{mag}, \bar{E}_{grad}$.

Weights are then chosen so that the contribution of each term to the total energy is of comparable order:

$$c \sim \frac{1}{\bar{E}_{con}}, d \sim \frac{1}{\bar{E}_{bal}}, g \sim \frac{1}{\bar{E}_{mag}}, h \sim \frac{1}{\bar{E}_{grad}}.$$

The entire set is then scaled by the common pair $a$, $b$ according to the desired contour “stiffness”.

**2 Coefficient ratios.** For contour evolution via gradient descent, what matters is not the absolute magnitude of the functional but the relative contribution of terms to its derivative. Therefore, it is preferable to tune the ratios of coefficients rather than their absolute values

The ratio $a{:}\,b$ shows how much stronger the internal energy is relative to the external energy. If $a \geq b$, the contour will be very smooth but will weakly respond to image details, increasing the risk of under-segmentation (the initial contour may not reach the real boundary). If $a \leq b$, the contour will aggressively track any gradients and contrasts, potentially leading to noise and false boundaries.

The ratio $c{:}\,d$ is the ratio of contour smoothness to balloon expansion capability. A large value of $c$ will cause the contour to tend toward a more uniform shape and contract quickly, potentially losing fine profile details. An excessively large value of $d$ may cause the contour to compress too aggressively.

The ratio $g{:}\,h$ governs sensitivity to brightness versus sensitivity to boundaries (gradient). Coefficient $g$ orients the contour toward regions of specific brightness (e.g., darker soft tissues against background). Coefficient $h$ orients the contour toward lines with maximum gradient magnitude (i.e., boundaries), which is critical for well-defined contours, especially in medical images with clear tissue transitions. In facial profile cephalometry, the soft-tissue boundary is typically well described by the gradient (skin-background contrast), so in practice it is advisable to choose $h > g$, placing the main emphasis on $E_{grad}$ and using the brightness term as an additional stabilizing component

## 5 Contour Analysis Algorithm for Cephalometric Tasks

Once the closed soft-tissue facial profile contour is obtained, the task reduces to finding extremal points – local maxima and minima corresponding to key cephalometric landmarks (nose tip, lips, chin, forehead, nasion, etc.). Computationally, this is a problem of analyzing a single-variable function defined on a closed curve. The following algorithm is proposed:

1. Transformation to polar coordinates.
2. Contour unrolling.
3. Finding extrema of the profile function.
4. Inverse transformation to Cartesian coordinates.
5. Correspondence of extrema to anatomical points.
6. Vector-angular analysis for profile type classification.
7. Assessment of profile harmony.

Let the closed contour after segmentation be parametrically defined as a set of points $A_k = (x_k, y_k)$, $k = 1, 2, \ldots, N$, arranged clockwise or counterclockwise. A reference center $O = (0, 0)$ is chosen. In this work, the center of the initial contour or the centroid of the detected profile is conveniently used as the center. Each contour point $A_k$ is converted to polar coordinates:

$$\varphi_k = arctg\ \left(\frac{y_k}{x_k}\right);\ \ \rho_k = \sqrt{x_k^2 + y_k^2}.$$

Here $\varphi_k$ is the angle between the $x$-axis and the radius vector connecting point $A_k$ with center $O$, and $\rho_k$ is the distance from the center to the point. In the context of this article $arctg\ (y_k/x_k)$ returns values in $(-\pi/2, \pi/2)$; the correct quadrant is determined by the signs of $x_k$ and $y_k$ according to the standard convention: $\varphi_k$ is adjusted by $(+\pi)$ if $x_k < 0$ and $y_k \geq 0$, by $(-\pi)$ if $x_k < 0$ and $y_k < 0$, and is undefined for $x_k = 0$. Points with $x_k = 0$ are handled as special cases with $\varphi_k = \pi/2$ if $y_k > 0$ and $\varphi_k = -\pi/2$ if $y_k < 0$.

Thus, the original two-dimensional contour $C$ is represented as a one-dimensional periodic function $\rho(\varphi) \approx \rho_k$ on a discrete set of angles $\{\varphi_k\}_{k=1}^{N}$. This unrolling converts the closed profile into a radius-versus-angle function defined on the interval $(-\pi, \pi]$ or $[0, 2\pi)$ with periodic boundary conditions.

The search for extrema of the profile function is performed to identify key cephalometric landmarks. Local maxima of $\rho(\varphi)$ correspond to the most prominent profile regions (nose tip, chin, forehead, lip vertices). Local minima correspond to the most recessed regions (subnasale area, nasion, etc.).

Computationally, finding local extrema of the discrete sequence $\{\rho_k\}$ is based on the following criterion: point with index $k$ is a local maximum of order $m$ if $\rho_k > \rho_{k-j}$ and $\rho_k > \rho_{k+j}$ for all $j = 1, 2, \ldots, m$. A local minimum is defined analogously.

The parameter $m$ defines the neighborhood size within which locality of the extremum is verified. Increasing m filters out small noise oscillations and retains only major, anatomically significant extrema.

Arrays of maxima and minima of the contour function are then formed and sorted by angle $\varphi$ in the traversal direction, with the starting point chosen as the extremum located to the right of and below the center of the initial contour – this fixes the baseline reference point on the profile.

For subsequent cephalometric analysis, all extremal points are converted back to the Cartesian coordinate system. For each extremum point $(\varphi_1, \rho_1)$, the coordinates are computed as:

$$x_2 = \rho_1 cos(\varphi_1) + x_c, \;\; y_2 = \rho_1 sin(\varphi_1) + y_c,$$

where $(x_c, y_c)$ are the coordinates of the initial contour center, accounting for any coordinate system shift relative to the source image. Each extremal point thus receives coordinates in the source image system.

The extrema are ordered so that the first element of the maxima array $A_1(x_1, y_1)$, located to the right of and below the center, corresponds to the nose tip. Continuing counterclockwise, the next three maxima $A_2(x_2, y_2)$, $A_3(x_3, y_3)$, $A_4(x_4, y_4)$ correspond to the upper lip, lower lip, and the most prominent point of the chin, respectively. The last maximum $A_5(x_5, y_5)$ corresponds to the most prominent point of the forehead. The first minimum $A_6(x_6, y_6)$ and the last minimum $A_7(x_7, y_7)$ correspond to the subnasale point and the nasion, respectively.

Thus, through strict ordering of the extrema and their positions relative to the center and to each other, an unambiguous correspondence is established between the mathematically detected extremal points and the clinically significant cephalometric landmarks (Fig. 2a).

Based on the identified points, line segments are formed from which the angles characterizing the profile type are calculated.

The angle characterizing the profile type is computed from vectors formed by the point pairs $(A_4, A_6)$ and $(A_5, A_6)$:

$$u = (m_1, n_1) = (x_6 - x_4, y_6 - y_4),$$

$$v = (m_2, n_2) = (x_6 - x_5, y_6 - y_5),$$

$$\varphi = arccos\left(\frac{m_1 m_2 + n_1 n_2}{\sqrt{m_1^2 + n_1^2} \cdot \sqrt{m_2^2 + n_2^2}}\right).$$

The resulting angle $\varphi$ is assessed against threshold values defining the acceptable variation range for a straight profile, accounting for anatomical variability and measurement errors (Fig. 2b):

- $170^{o} \leq \varphi \leq 190^{o}$ – straight profile;
- $\varphi < 170^{o}$– convex profile;
- $\varphi > 190^{o}$– concave profile.

The Ricketts aesthetic line is defined as the line passing through points $A_1(x_1, y_1)$ and $A_4(x_4, y_4)$, corresponding to the nose tip and the most prominent point of the chin. The equation of this line can be written as:

$$\frac{x - x_1}{x_4 - x_1} = \frac{y - y_1}{y_4 - y_1},$$

or in general form: $ax + by + c = 0$. For the lip points $A_2(x_2, y_2)$ and $A_3(x_3, y_3)$, the signs and magnitudes of algebraic distances to this line are computed. If both points are on the same side of the line and do not lie on it or cross it (e.g., they are posterior by no more than a specified threshold), the profile is considered harmoniously developed; otherwise, the profile is considered disharmonious (Fig. 2c).

# 6 Experimental Results

The dataset consists exclusively of profile-view photographs; automated processing of frontal (en-face) images does not present significant methodological challenges and is not the focus of this study. Standard side-profile photographs taken under controlled lighting conditions against a uniform, neutral background were selected for processing. The images were taken from a publicly available face image dataset. The 120 images are evenly distributed across three profile types: 40 images per class (straight, convex, concave). Prior to annotation, all images underwent a standardized pre-processing pipeline: cropping to the facial bounding box detected by a Haar cascade classifier; conversion to grayscale; rescaling to a uniform resolution; noise removal using morphological operations (erosion, dilation, opening, closing, and logical filters); contrast enhancement; blurring via the Inverse Gaussian Gradient. After pre-processing, all images were annotated in two independent ways: automatically using the proposed algorithm, and manually by a medical specialist serving as ground truth. In both cases, three annotation tasks were performed: localization of seven key cephalometric landmarks; multi-class profile type classification (straight/convex/concave); binary harmony assessment.

Automatic annotation accuracy was evaluated using three metrics:

**1 Localization accuracy of seven key cephalometric points.** The mean displacement $\sigma$ of automatically detected points $(x_j, y_j)$ from reference points $(x_i, y_i)$ was used as the metric:

$$\sigma = \frac{1}{7\,N} \sum_{i,j=1}^{7} \sqrt{\left(x_j - x_i\right)^2 + \left(y_j - y_i\right)^2}.$$

**2 Multi-class profile type classification accuracy.** The fraction of incorrect decisions when assigning the profile to one of three classes (straight, convex, concave) was evaluated. The indicator $P_{type}$ was used as the misclassification probability.

**3 Binary profile harmony assessment accuracy** $P_{harm}$ was evaluated analogously as the fraction of incorrect answers when determining profile harmony.

Experiments were conducted with different sets of weighting coefficients governing the contributions of contour smoothing energy, balloon energy, and gradient energy. For each set, $\sigma$, $P_{type}$, and $P_{harm}$ were computed (Table 1).

To assess the statistical robustness of results, 95% confidence intervals for classification indicators were constructed for each set of weighting coefficients. Since $P_{type}$ and $P_{harm}$ represent sample proportions at $N = 120$, the Wilson score interval was applied for interval estimation (preferred over the normal approximation for small samples and extreme proportion values):

$$CI_{95\%}(\hat{p}) = \frac{\hat{p}+\frac{z^2}{2N}\pm z\sqrt{\frac{\hat{p}(1-\hat{p})}{N}+\frac{z^2}{4N^2}}}{1+\frac{z^2}{N}}, \qquad z = 1.96.$$

The anomalous result in row 2 ($P_{harm} = 0.97$ despite $P_{type} = 0.11$) is explained by the increased smoothing coefficient $E_{con} = 0.02$: the higher contour stiffness preserves major extrema (nose tip, chin, forehead) used for profile type assessment, but suppresses the smaller lip-vertex extrema ($A_2, A_3$) critical for Ricketts line computation, leading to systematic failure of harmony assessment.

A statistically significant negative result is $P_{harm} = 0.97$ with confidence interval [0.922; 0.989]. For this parameter set, profile harmony is incorrectly determined in almost all cases, since the confidence interval lies entirely in the region of high errors.

Values $P_{type} = 0.02$ и $P_{harm} = 0.03$ were obtained with optimal coefficient selection. In this case, the upper bound of the confidence intervals for both indicators does not exceed 0.08, which is clinically interpreted as acceptable accuracy for automated primary annotation tasks.

At relatively high coefficient values, the internal and external energies form a contour that may be insufficiently stable: localization accuracy $\sigma$ for key cephalometric landmarks remains relatively high, while misclassification probabilities for profile type and harmony vary strongly depending on the balance between smoothing and gradient.

Table 1 Experimental results for different sets of weighting coefficients.

| **Values of the coefficients corresponding to the energy functions** | | | **Localization accuracy** | **Probability of automatic misclassification / confidence interval** | |
|---|---|---|---|---|---|
| $E_{con}$ | $E_{bal}$ | $E_{grad}$ | $\sigma$ | $P_{type}$ **[95% CI]** | $P_{harm}$ **[95% CI]** |
| 0.01 | 0.01 | 0.01 | 29.76 | 0.64 [0.551; 0.720] | 0.12 [0.073; 0.190] |
| 0.02 | 0.01 | 0.01 | 25.27 | 0.11 [0.066; 0.179] | 0.97 [0.922; 0.989] |
| 0.05 | 0.01 | 0.01 | 37.41 | 0.08 [0.044; 0.143] | 0.86 [0.787; 0.911] |
| 0.01 | 0.01 | 0.05 | 26.83 | 0.48 [0.393; 0.569] | 0.09 [0.051; 0.155] |
| 0.001 | 0.001 | 0.005 | 74.35 | 0.98 [0.936; 0.994] | 0.23 [0.164; 0.313] |
| 0.001 | 0.001 | 0.001 | 3.66 | 0.02 [0.006; 0.064] | 0.03 [0.011; 0.078] |

(a) (b) (c)

Fig. 2 Results of automatic processing of a profile photograph: (a) extracted soft-tissue contour (blue) with detected extrema – maxima (cyan dots) and minima (yellow dots); initial circular contour shown in red dashed line; (b) profile type assessment – lines through landmarks Gl, Sn, Pg (blue dots) with the computed angle $\varphi$; (c) Ricketts aesthetic line through the nose tip and pogonion with lip position (blue dots).

 doi: 10.18287/JBPE26.12.020309

However, at optimal energy parameters, the error in detecting key landmarks becomes sufficiently small, the discrepancy between automatic and manual classification of profile type and harmony is minimal and clinically negligible. This means the method can be used for automated primary annotation of large datasets, preparation of training samples for neural network models, and as an auxiliary tool in clinical decision support systems in orthodontics (Fig. 2).

For reference, landmark localization errors reported for CNN-based methods on similar cephalometric tasks range from 1.5 to 6 px [11, 12], which is comparable to the $\sigma = 3.66$ px achieved by the proposed training-free variational approach.

## 7 Conclusion

The results obtained confirm the applicability of the proposed variational active contour method to the task of automated biomedical image processing of the soft-tissue facial profile. With optimal selection of the energy functional weighting coefficients, the algorithm achieves a mean displacement of key cephalometric landmarks $\sigma = 3.66$ px and misclassification probabilities for profile type and harmony not exceeding 0.03 – which is clinically interpreted as acceptable accuracy for primary automatic annotation systems.

From a clinical application perspective, the proposed method can be used to accelerate medical documentation, reduce the workload of the orthodontist during screening examinations, and for standardized preparation of annotated training datasets for the development of neural network models for cephalometric feature recognition. The ability to operate without prior training on annotated data distinguishes the proposed variational approach from dominant deep learning methods and makes it suitable for clinical institutions with limited archival data.

Future development of the method is promising in the direction of adaptive parameter tuning of active contours for image type and quality, integration with three-dimensional craniofacial models, and closer combination with deep learning methods – including within hybrid architectures combining variational segmentation and neural network classification of biomedical images.

The proposed method does not rely on dataset-specific training and operates on standard profile photographs with uniform background; its applicability to images with cluttered backgrounds or non-standard lighting may require adjustment of the gradient energy weight $h$.

Results obtained in similar biomedical segmentation tasks using CNN and hybrid DL models, as well as experience in localizing anatomical landmarks in craniofacial images, confirm the potential of integrating the variational approach with modern deep learning methods [11–13].

## Disclosures

The authors declare no conflicts of interest in this paper.

## References


1. I. V. Tokarevich, N. V. Korkhova, I. V. Moskaleva, L. V. Kipkaeva, T. V. Terekhova, D. V. Khandogiy, Yu.Ya. Naumovich, and S. S. Denisov, General Orthodontics, BSMU, Minsk (2015). ISBN: 978-985-567-355-3.[in Russian]
2. P. Farha, S. A. Arqub, and M. S. Ghoussoub, "Correlation between cephalometric values and soft tissue profile in class I and class II adult patients based on vertical patterns," Turkish Journal of Orthodontics 37(1), 36-43 (2024).
3. S. Pandey, S. Kapoor, S. Agarwal, and I. Shukla, "Evaluation of lip position in esthetically pleasing profiles using different reference lines: a photographic study," Journal of Indian Orthodontic Society 55(3), 261-269 (2021).
4. Y. Chen, P. Ge, G. Wang, G. Weng, and H. Chen, "An overview of intelligent image segmentation using active contour models," Intelligence & Robotics 3(1), 23–55 (2023).
5. F. Pierre, M. Amendola, C. Bigeard, T. Ruel, and P.-F. Villard, "Segmentation with Active Contours," Image Processing On Line 11, 120–141 (2021).
6. Z. Wang, N. Li, Q. Zhang, J. Wei, L. Zhang, and Y. Wang, "Directionally weakened diffusion for image segmentation using active contours," Frontiers in Applied Mathematics and Statistics 9, 1275588 (2023).
7. A. A. Memon, S. Soomro, M. T. Shahid, A. Munir, A. Niaz, and K. N. Choi, "Segmentation of Intensity-Corrupted Medical Images Using Adaptive Weight-Based Hybrid Active Contours," Computational and Mathematical Methods in Medicine 2020, 317415 (2020).
8. P. Viola, M. J. Jones, "Robust Real-Time Face Detection," International Journal of Computer Vision 57(2), 137–154 (2004).
9. V. Kazemi, J. Sullivan, "One millisecond face alignment with an ensemble of regression trees," in Proceedings of the IEEE conference on computer vision and pattern recognition, 1867-1874 (2014).
10. A. Joshi, M. S. Khan, A. Niaz, F. Akram, H. C. Song, and K. N. Choi, "Active contour model with adaptive weighted function for robust image segmentation under biased conditions," Expert Systems with Applications 175, 114811 (2021).
11. A. H. Jalalzadeh, M. H. Kamangar, "A Hybrid Super-Resolution Method for Medical Images Using Transfer Learning," Journal of Biomedical Photonics & Engineering 11(4), 040304 (2025).

12. B. A. R., V. K. R. S., and K. S. S., "The Implications of Varying Batch-Size in the Classification of Patch-Based Lung Nodules Using Convolutional Neural Network Architecture on Computed Tomography Images," Journal of Biomedical Photonics & Engineering 10(1), 010305 (2024).
13. I. Shchechkin, S. Rodimova, A. Mozherov, V. Elagin, N. Bobrov, V. Shcheslavsky, V. Zagainov, E. Zagaynova, and D. Kuznetsova, "Neural Networks for Medical Data Processing: Segmentation of Fluorescence Lifetime Imaging Microscopy," Journal of Biomedical Photonics & Engineering 11(3), 030304 (2025).